Measurements of mass-dependent azimuthal anisotropy in central p+Au, d+Au, and 3He+Au collisions at √sNN=200 GeV

Adare, A.; ...; Makek, Mihael; ...; Vukman, Nikola; ...; Zou, L.

Source / Izvornik: **Physical Review C, 2018, 97**

Journal article, Published version
Rad u časopisu, Objavljena verzija rada (izdavačev PDF)

https://doi.org/10.1103/PhysRevC.97.064904

Permanent link / Trajna poveznica: https://urn.nsk.hr/urn:nbn:hr:217:311198

Rights / Prava: In copyright / Zaštićeno autorskim pravom.

Download date / Datum preuzimanja: **2024-03-29**



Repository / Repozitorij:

Repository of the Faculty of Science - University of Zagreb





Measurements of mass-dependent azimuthal anisotropy in central p + Au, d + Au, and ^{3}He + Au collisions at $\sqrt{s_{NN}} = 200$ GeV

A. Adare,[13] C. Aidala,[41] N. N. Ajitanand,[57,*] Y. Akiba,[52,53,†] M. Alfred,[23] V. Andrieux,[41] N. Apadula,[28,58] H. Asano,[34,52] B. Azmoun,[7] V. Babintsev,[24] A. Bagoly,[17] M. Bai,[6] N. S. Bandara,[40] B. Bannier,[58] K. N. Barish,[8] S. Bathe,[5,53] A. Bazilevsky,[7] M. Beaumier,[8] S. Beckman,[13] R. Belmont,[13,41] A. Berdnikov,[55] Y. Berdnikov,[55] D. S. Blau,[33,44] M. Boer,[36] J. S. Bok,[46] K. Boyle,[53] M. L. Brooks,[36] J. Bryslawskyj,[5,8] V. Bumazhnov,[24] S. Campbell,[14,28] V. Canoa Roman,[58] R. Cervantes,[58] C.-H. Chen,[53] C. Y. Chi,[14] M. Chiu,[7] I. J. Choi,[25] J. B. Choi,[10,*] T. Chujo,[61] Z. Citron,[63] M. Connors,[21,53] N. Cronin,[42,58] M. Csanád,[17] T. Csörgő,[18,64] T. W. Danley,[47] A. Datta,[45] M. S. Daugherity,[1] G. David,[7,58] K. DeBlasio,[45] K. Dehmelt,[58] A. Denisov,[24] A. Deshpande,[53,58] E. J. Desmond,[7] A. Dion,[58] P. B. Diss,[39] D. Dixit,[58] J. H. Do,[65] A. Drees,[58] K. A. Drees,[6] J. M. Durham,[36] A. Durum,[24] A. Enokizono,[52,54] H. En'yo,[52] S. Esumi,[61] B. Fadem,[42] W. Fan,[58] N. Feege,[58] D. E. Fields,[45] M. Finger,[9] M. Finger, Jr.,[9] S. L. Fokin,[33] J. E. Frantz,[47] A. Franz,[7] A. D. Frawley,[20] Y. Fukuda,[61] C. Gal,[58] P. Gallus,[15] P. Garg,[3,58] H. Ge,[58] F. Giordano,[25] A. Glenn,[35] Y. Goto,[52,53] N. Grau,[2] S. V. Greene,[62] M. Grosse Perdekamp,[25] T. Gunji,[12] H. Guragain,[21] T. Hachiya,[52,53] J. S. Haggerty,[7] K. I. Hahn,[19] H. Hamagaki,[12] H. F. Hamilton,[1] S. Y. Han,[19] J. Hanks,[58] S. Hasegawa,[29] T. O. S. Haseler,[21] K. Hashimoto,[52,54] X. He,[21] T. K. Hemmick,[58] J. C. Hill,[28] K. Hill,[13] A. Hodges,[21] R. S. Hollis,[8] K. Homma,[22] B. Hong,[32] T. Hoshino,[22] N. Hotvedt,[28] J. Huang,[7] S. Huang,[62] K. Imai,[29] J. Imrek,[16] M. Inaba,[61] A. Iordanova,[8] D. Isenhower,[1] D. Ivanishchev,[51] B. V. Jacak,[58] M. Jezghani,[21] Z. Ji,[58] J. Jia,[7,57] X. Jiang,[36] B. M. Johnson,[7,21] V. Jorjadze,[58] D. Jouan,[49] D. S. Jumper,[25] S. Kanda,[12] J. H. Kang,[65] D. Kapukchyan,[8] S. Karthas,[58] D. Kawall,[40] A. V. Kazantsev,[33] J. A. Key,[45] V. Khachatryan,[58] A. Khanzadeev,[51] C. Kim,[8,32] D. J. Kim,[30] E.-J. Kim,[10] G. W. Kim,[19] M. Kim,[56] M. H. Kim,[32] B. Kimelman,[42] D. Kincses,[17] E. Kistenev,[7] R. Kitamura,[12] J. Klatsky,[20] D. Kleinjan,[8] P. Kline,[58] T. Koblesky,[13] B. Komkov,[51] D. Kotov,[51,55] S. Kudo,[61] B. Kurgyis,[17] K. Kurita,[54] M. Kurosawa,[52,53] Y. Kwon,[65] R. Lacey,[57] J. G. Lajoie,[28] A. Lebedev,[28] S. Lee,[65] S. H. Lee,[28,58] M. J. Leitch,[36] Y. H. Leung,[58] N. A. Lewis,[41] X. Li,[11] X. Li,[36] S. H. Lim,[36,65] M. X. Liu,[36] V.-R. Loggins,[25] S. Lökös,[17,18] K. Lovasz,[16] D. Lynch,[7] T. Majoros,[16] Y. I. Makdisi,[6] M. Makek,[66] A. Manion,[58] V. I. Manko,[33] E. Mannel,[7] H. Masuda,[54] M. McCumber,[36] P. L. McGaughey,[36] D. McGlinchey,[13,36] C. McKinney,[25] A. Meles,[46] M. Mendoza,[8] W. J. Metzger,[18] A. C. Mignerey,[39] D. E. Mihalik,[58] A. Milov,[63] D. K. Mishra,[4] J. T. Mitchell,[7] G. Mitsuka,[53] S. Miyasaka,[52,60] S. Mizuno,[52,61] A. K. Mohanty,[4] P. Montuenga,[25] T. Moon,[65] D. P. Morrison,[7] S. I. Morrow,[62] T. V. Moukhanova,[33] T. Murakami,[34,52] J. Murata,[52,54] A. Mwai,[57] K. Nagai,[60] K. Nagashima,[22] T. Nagashima,[54] J. L. Nagle,[13] M. I. Nagy,[17] I. Nakagawa,[52,53] H. Nakagomi,[52,61] K. Nakano,[52,60] C. Nattrass,[59] P. K. Netrakanti,[4] T. Niida,[61] S. Nishimura,[12] R. Nouicer,[7,53] T. Novák,[18,64] N. Novitzky,[30,58] A. S. Nyanin,[33] E. O'Brien,[7] C. A. Ogilvie,[28] J. D. Orjuela Koop,[13] J. D. Osborn,[41] A. Oskarsson,[37] G. J. Ottino,[45] K. Ozawa,[31,61] R. Pak,[7] V. Pantuev,[26] V. Papavassiliou,[46] J. S. Park,[56] S. Park,[52,56,58] S. F. Pate,[46] M. Patel,[28] J.-C. Peng,[25] W. Peng,[62] D. V. Perepelitsa,[7,13] G. D. N. Perera,[46] D. Yu. Peressounko,[33] C. E. PerezLara,[58] J. Perry,[28] R. Petti,[7,58] M. Phipps,[7,25] C. Pinkenburg,[7] R. Pinson,[1] R. P. Pisani,[7] A. Pun,[47] M. L. Purschke,[7] P. V. Radzevich,[55] J. Rak,[30] B. J. Ramson,[41] I. Ravinovich,[63] K. F. Read,[48,59] D. Reynolds,[57] V. Riabov,[44,51] Y. Riabov,[51,55] D. Richford,[5] T. Rinn,[28] S. D. Rolnick,[8] M. Rosati,[28] Z. Rowan,[5] J. G. Rubin,[41] J. Runchey,[28] A. S. Safonov,[55] B. Sahlmueller,[58] N. Saito,[31] T. Sakaguchi,[7] H. Sako,[29] V. Samsonov,[44,51] M. Sarsour,[21] K. Sato,[61] S. Sato,[29] B. Schaefer,[62] B. K. Schmoll,[59] K. Sedgwick,[8] R. Seidl,[52,53] A. Sen,[28,59] R. Seto,[8] P. Sett,[4] A. Sexton,[39] D. Sharma,[58] I. Shein,[24] T.-A. Shibata,[52,60] K. Shigaki,[22] M. Shimomura,[28,43] T. Shioya,[61] P. Shukla,[4] A. Sickles,[7,25] C. L. Silva,[36] D. Silvermyr,[37,48] B. K. Singh,[3] C. P. Singh,[3] V. Singh,[3] M. J. Skoby,[41] M. Slunečka,[9] M. Snowball,[36] R. A. Soltz,[35] W. E. Sondheim,[36] S. P. Sorensen,[59] I. V. Sourikova,[7] P. W. Stankus,[48] M. Stepanov,[40,*] S. P. Stoll,[7] T. Sugitate,[22] A. Sukhanov,[7] T. Sumita,[52] J. Sun,[58] J. Sziklai,[64] A. Takeda,[43] A. Taketani,[52,53] K. Tanida,[29,53,56] M. J. Tannenbaum,[7] S. Tarafdar,[62,63] A. Taranenko,[44,57] G. Tarnai,[16] R. Tieulent,[21,38] A. Timilsina,[28] T. Todoroki,[52,61] M. Tomášek,[15] C. L. Towell,[1] R. Towell,[1] R. S. Towell,[1] I. Tserruya,[63] Y. Ueda,[22] B. Ujvari,[16] H. W. van Hecke,[36] S. Vazquez-Carson,[13] J. Velkovska,[62] M. Virius,[15] V. Vrba,[15,27] N. Vukman,[66] X. R. Wang,[46,53] Z. Wang,[5] Y. Watanabe,[52,53] Y. S. Watanabe,[12,31] F. Wei,[46] A. S. White,[41] C. P. Wong,[21] C. L. Woody,[7] M. Wysocki,[48] B. Xia,[47] C. Xu,[46] Q. Xu,[62] L. Xue,[21] S. Yalcin,[58] Y. L. Yamaguchi,[12,53,58] H. Yamamoto,[61] A. Yanovich,[24] P. Yin,[13] J. H. Yoo,[32] I. Yoon,[56] H. Yu,[46,50] I. E. Yushmanov,[33] W. A. Zajc,[14] A. Zelenski,[6] S. Zharko,[55] S. Zhou,[11] and L. Zou[8]

(PHENIX Collaboration)

[1]*Abilene Christian University, Abilene, Texas 79699, USA*

[2]*Department of Physics, Augustana University, Sioux Falls, South Dakota 57197, USA*

[3]*Department of Physics, Banaras Hindu University, Varanasi 221005, India*

[4]*Bhabha Atomic Research Centre, Bombay 400 085, India*

[5]*Baruch College, City University of New York, New York, New York 10010, USA*

[6]*Collider-Accelerator Department, Brookhaven National Laboratory, Upton, New York 11973-5000, USA*

[7]*Physics Department, Brookhaven National Laboratory, Upton, New York 11973-5000, USA*

[8]*University of California-Riverside, Riverside, California 92521, USA*

[9]*Charles University, Ovocný trh 5, Praha 1, 116 36, Prague, Czech Republic*

 ©2018 American Physical Society

[10]*Chonbuk National University, Jeonju, 561-756, Korea*
[11]*Science and Technology on Nuclear Data Laboratory, China Institute of Atomic Energy, Beijing 102413, People's Republic of China*
[12]*Center for Nuclear Study, Graduate School of Science, University of Tokyo, 7-3-1 Hongo, Bunkyo, Tokyo 113-0033, Japan*
[13]*University of Colorado, Boulder, Colorado 80309, USA*
[14]*Columbia University, New York, New York 10027 and Nevis Laboratories, Irvington, New York 10533, USA*
[15]*Czech Technical University, Zikova 4, 166 36 Prague 6, Czech Republic*
[16]*Debrecen University, H-4010 Debrecen, Egyetem tér 1, Hungary*
[17]*ELTE, Eötvös Loránd University, H-1117 Budapest, Pázmány P. s. 1/A, Hungary*
[18]*Eszterházy Károly University, Károly Róbert Campus, H-3200 Gyöngyös, Mátrai út 36, Hungary*
[19]*Ewha Womans University, Seoul 120-750, Korea*
[20]*Florida State University, Tallahassee, Florida 32306, USA*
[21]*Georgia State University, Atlanta, Georgia 30303, USA*
[22]*Hiroshima University, Kagamiyama, Higashi-Hiroshima 739-8526, Japan*
[23]*Department of Physics and Astronomy, Howard University, Washington, DC 20059, USA*
[24]*IHEP Protvino, State Research Center of Russian Federation, Institute for High Energy Physics, Protvino, 142281, Russia*
[25]*University of Illinois at Urbana-Champaign, Urbana, Illinois 61801, USA*
[26]*Institute for Nuclear Research of the Russian Academy of Sciences, prospekt 60-letiya Oktyabrya 7a, Moscow 117312, Russia*
[27]*Institute of Physics, Academy of Sciences of the Czech Republic, Na Slovance 2, 182 21 Prague 8, Czech Republic*
[28]*Iowa State University, Ames, Iowa 50011, USA*
[29]*Advanced Science Research Center, Japan Atomic Energy Agency, 2-4 Shirakata Shirane, Tokai-mura, Naka-gun, Ibaraki-ken 319-1195, Japan*
[30]*Helsinki Institute of Physics and University of Jyväskylä, P.O.Box 35, FI-40014 Jyväskylä, Finland*
[31]*KEK, High Energy Accelerator Research Organization, Tsukuba, Ibaraki 305-0801, Japan*
[32]*Korea University, Seoul, 136-701, Korea*
[33]*National Research Center "Kurchatov Institute," Moscow, 123098, Russia*
[34]*Kyoto University, Kyoto 606-8502, Japan*
[35]*Lawrence Livermore National Laboratory, Livermore, California 94550, USA*
[36]*Los Alamos National Laboratory, Los Alamos, New Mexico 87545, USA*
[37]*Department of Physics, Lund University, Box 118, SE-221 00 Lund, Sweden*
[38]*IPNL, CNRS/IN2P3, Univ Lyon, Université Lyon 1, F-69622, Villeurbanne, France*
[39]*University of Maryland, College Park, Maryland 20742, USA*
[40]*Department of Physics, University of Massachusetts, Amherst, Massachusetts 01003-9337, USA*
[41]*Department of Physics, University of Michigan, Ann Arbor, Michigan 48109-1040, USA*
[42]*Muhlenberg College, Allentown, Pennsylvania 18104-5586, USA*
[43]*Nara Women's University, Kita-uoya Nishi-machi Nara 630-8506, Japan*
[44]*National Research Nuclear University, MEPhI, Moscow Engineering Physics Institute, Moscow 115409, Russia*
[45]*University of New Mexico, Albuquerque, New Mexico 87131, USA*
[46]*New Mexico State University, Las Cruces, New Mexico 88003, USA*
[47]*Department of Physics and Astronomy, Ohio University, Athens, Ohio 45701, USA*
[48]*Oak Ridge National Laboratory, Oak Ridge, Tennessee 37831, USA*
[49]*IPN-Orsay, Univ. Paris-Sud, CNRS/IN2P3, Université Paris-Saclay, BP1, F-91406, Orsay, France*
[50]*Peking University, Beijing 100871, People's Republic of China*
[51]*PNPI, Petersburg Nuclear Physics Institute, Gatchina, Leningrad region, 188300, Russia*
[52]*RIKEN Nishina Center for Accelerator-Based Science, Wako, Saitama 351-0198, Japan*
[53]*RIKEN BNL Research Center, Brookhaven National Laboratory, Upton, New York 11973-5000, USA*
[54]*Physics Department, Rikkyo University, 3-34-1 Nishi-Ikebukuro, Toshima, Tokyo 171-8501, Japan*
[55]*Saint Petersburg State Polytechnic University, St. Petersburg, 195251, Russia*
[56]*Department of Physics and Astronomy, Seoul National University, Seoul 151-742, Korea*
[57]*Chemistry Department, Stony Brook University, SUNY, Stony Brook, New York 11794-3400, USA*
[58]*Department of Physics and Astronomy, Stony Brook University, SUNY, Stony Brook, New York 11794-3800, USA*
[59]*University of Tennessee, Knoxville, Tennessee 37996, USA*
[60]*Department of Physics, Tokyo Institute of Technology, Oh-okayama, Meguro, Tokyo 152-8551, Japan*
[61]*Tomonaga Center for the History of the Universe, University of Tsukuba, Tsukuba, Ibaraki 305, Japan*
[62]*Vanderbilt University, Nashville, Tennessee 37235, USA*
[63]*Weizmann Institute, Rehovot 76100, Israel*
[64]*Institute for Particle and Nuclear Physics, Wigner Research Centre for Physics, Hungarian Academy of Sciences (Wigner RCP, RMKI) H-1525 Budapest 114, POBox 49, Budapest, Hungary*
[65]*Yonsei University, IPAP, Seoul 120-749, Korea*
[66]*Department of Physics, Faculty of Science, University of Zagreb, Bijenička c. 32 HR-10002 Zagreb, Croatia*

(Received 27 October 2017; published 11 June 2018)

We present measurements of the transverse-momentum dependence of elliptic flow v_2 for identified pions and (anti)protons at midrapidity ($|\eta| < 0.35$), in 0%–5% central $p+$Au and ^{3}He + Au collisions at $\sqrt{s_{NN}} =$ 200 GeV. When taken together with previously published measurements in $d+$Au collisions at $\sqrt{s_{NN}} =$ 200 GeV, the results cover a broad range of small-collision-system multiplicities and intrinsic initial geometries. We observe a clear mass-dependent splitting of $v_2(p_T)$ in $d+$Au and ^{3}He + Au collisions, just as in large nucleus-nucleus ($A+A$) collisions, and a smaller splitting in $p+$Au collisions. Both hydrodynamic and transport model calculations successfully describe the data at low p_T (<1.5 GeV/c), but fail to describe various features at higher p_T. In all systems, the v_2 values follow an approximate quark-number scaling as a function of the hadron transverse kinetic energy per constituent quark (KE_T/n_q), which was also seen previously in $A+A$ collisions.

DOI: 10.1103/PhysRevC.97.064904

I. INTRODUCTION

Recent years have seen a paradigm shift in our understanding of the minimum conditions required for the production of the quark-gluon plasma (QGP). In large nucleus-nucleus ($A+A$) collisions, signals of collective behavior—such as the azimuthal momentum anisotropy of final-state particles relative to the event plane—have been successfully understood in the context of nearly inviscid hydrodynamic calculations, thus establishing the notion of a strongly interacting, nearly perfect fluid being formed in this class of collisions [1].

However, the discovery of the same azimuthal anisotropy signals in a variety of small collision systems (i.e, p,d,^{3}He+Au at $\sqrt{s_{NN}} = 200$ GeV [2–4]; $p+$Pb at $\sqrt{s_{NN}} =$ 5.02 TeV; $p+p$ at $\sqrt{s} = 2.76$, 5.02, and 13 TeV [5–11]; and an earlier observation of long-range two-particle correlations in $p+p$ collisions at $\sqrt{s} = 7$ TeV [10]) pose a challenge. It was believed that the system size in this class of collisions is too small to create any significant amount of hot nuclear matter, which in any case would be very short lived. There are also alternative explanations for these anisotropy signals based on momentum space domains and color recombination, such as in [12,13], although they lack quantitative predictions for small-system observables at the BNL Relativistic Heavy Ion Collider (RHIC). Therefore, in small collision systems, the identification of collective behavior with the hydrodynamic expansion of any potential QGP requires further scrutiny.

Measurements of elliptic and triangular flow (v_2, v_3) at RHIC in ^{3}He + Au collisions, as well as of v_2 in $d+$Au and $p+$Au collisions, demonstrated that the observed collective response in small collision systems is directly correlated with the event geometry [3,4,14], just as in $A+A$ collisions where the geometric configuration of the overlapping nuclei determines the pressure gradients that drive the expansion of the resulting QGP. Viscous hydrodynamic calculations successfully describe the measurements in the geometry-controlled experiments at RHIC [15–18], as well as those made at the CERN Large Hadron Collider (LHC) in $p+$Pb, and even in $p+p$ collisions [19]. The success of hydrodynamics in describing small-system collectivity over such a wide range of energies and for a variety of systems is taken as evidence for the claim that the QGP is formed in these collisions and through its expansion translates initial geometry into final-state momentum anisotropy.

If collectivity in small systems can indeed be understood as arising from the expansion of QGP droplets along pressure gradients determined by geometry, there should necessarily be a mass ordering of $v_2(p_T)$ for identified final-state hadrons. Strong radial expansion in the hydrodynamic evolution results in a shifting of the anisotropy pattern to higher p_T for higher mass hadrons due to a common velocity boost [1]. This fingerprint of hydrodynamic expansion on the $v_2(m, p_T)$ is one of the key signatures of the nearly inviscid fluid nature of the QGP formed in $A+A$ collisions; see for example [20]. Recently, such mass ordering has been observed in $d+$Au collisions at RHIC [3] and in $p+$Pb collisions at the LHC [21,22].

It is notable that a multiphase transport model (AMPT), an instance of a broader family of kinetic transport models [23], also finds a mass ordering of $v_2(p_T)$ in both $A+A$ and small systems, despite having only a modest number of parton scatterings and thus nothing close to a radial velocity field as in hydrodynamics [24]. Within AMPT the mass ordering is found to arise from the hadronic rescattering phase, after all partons have coalesced into hadrons, incorporating the different inelastic cross sections for different hadrons [24]. There are other approaches with fragmentation of saturated gluon states [25] and with color strings followed by hydrodynamics [26] that achieve some degree of mass ordering, though currently lacking in any predictions for small systems at RHIC energies.

The present study completes the set of small-system projectile geometry results at top RHIC energy by providing v_2 measurements for pions and (anti)protons (henceforth referred to as "protons") in central $p+$Au and ^{3}He + Au collisions at $\sqrt{s_{NN}} = 200$ GeV, and compares to v_2 measurements for pions and (anti)protons in central $d+$Au collisions at the same energy [3]. Detailed comparisons are then made with theory calculations from viscous hydrodynamics, as encoded in the SUPERSONIC [27] and the iEBE-VISHNU models [18], and the kinetic transport model AMPT.

II. METHODS

The PHENIX collaboration has measured the $v_2(p_T)$ of identified particles in $p+$Au, $d+$Au, and ^{3}He + Au collisions. We apply the same analysis procedure to all three

*Deceased.
†PHENIX spokesperson: akiba@rcf.rhic.bnl.gov

systems in the same centrality class to provide a controlled comparison from which to draw conclusions.

A complete description of the PHENIX detector and its subsystems can be found in [28,29]. Charged particles are reconstructed with the two central arm spectrometers, comprising drift chambers (DCs) and multiwire proportional pad chambers (PCs). Each arm covers an acceptance of $|\eta| < 0.35$ in pseudorapidity and $\pi/2$ in azimuth. Tracks in the drift chamber are matched to hits in the outer detectors. The distribution of differences between hits and projections is approximately Gaussian, with an additional underlying background caused by random associations. To suppress background from particle weak decays and photon conversions, tracks reconstructed with the DCs and the first layer of PCs are required to be matched to the third layer of PCs within three σ in the longitudinal and transverse planes, where p_T and charge sign dependent σ values are determined from Gaussian fits to residual distributions between PC clusters and the tracks extrapolated to the PC surface. Particle identification is performed using the time-of-flight (TOF) subsystem, which comprises two separate arms (east and west), constructed using scintillators [30] and multigap resistive plate chambers [31], and covers $\pi/4$ and $\pi/8$, respectively. The timing resolutions for the east and west TOF are 130 ps and 95 ps, respectively. Particle identification (PID) is based on the particle mass with p_T-dependent selections in mass-squared calculated using the particle momentum, time of flight, and path length. After track matching and PID selections, some residual background remains in the proton sample at low p_T (<1 GeV/c). In this p_T range, up to 15% of the reconstructed protons are secondary particles that originate from interactions of energetic particles produced in the collisions with detector material, primarily the silicon vertex tracker (VTX), which covers the pseudorapidity range $|\eta| < 1.2$. Detector simulations using GEANT3 [32] indicate that the contamination in the proton sample is negligible for $p_T > 1$ GeV/c, not present in the antiproton distributions, and negligible in the charged-pion sample at all p_T. To remove the background in the proton sample, the VTX detector [33] is used in conjunction with the DC to select proton tracks with $p_T < 1$ GeV/c based on their distance of closest approach (DCA) to the primary vertex in the x-y plane transverse to the beam direction. The tracks are required to be within two standard deviations of the mean value of the DCA distribution. This additional selection is not applied at higher p_T nor for particle species for which the secondary-particle contamination is negligible. The pions and protons selected for the analysis are identified with purity of over 98% for p_T up to 3 GeV/c in all collision systems.

The beam-beam counters (BBCs) comprise two arrays of 64 quartz radiator Čerenkov detectors, placed longitudinally ± 1.44 m away from the center of the interaction region (IR), covering $3.0 < |\eta| < 3.9$ and 2π in azimuth. The forward vertex detector (FVTX) is a silicon detector comprised of two identical end-cap assemblies symmetrically arranged in the longitudinal direction around the IR, covering the pseudorapidity acceptance $1.0 < |\eta| < 3.0$. Using hit clusters, it can detect charged particles with an efficiency greater than 95%. The arms of the BBC and FVTX in the Au-going direction (i.e., $\eta < 0$) are designated as the *south* arms and designated BBC-S and FVTX-S, respectively. We use the south arm of each of these detectors to determine the event plane of the collision. In addition, timing information from the BBC is used to determine the z vertex of the collision. In this analysis, a ± 10 cm cut on the collision z vertex is applied.

The $p+$Au data set for this analysis, taken during the 2015 run at RHIC, comprises 0.84×10^9 minimum-bias (MB) triggered events and 1.4×10^9 high-multiplicity (HM) triggered events. The MB trigger is defined as a coincidence in the same event between both arms of the BBC detector [34], requiring that at least one photomultiplier tube (PMT) fire in each. This definition allows $84 \pm 4\%$ of the total inelastic $p+$Au cross section to be captured. The HM trigger is based on the MB trigger, but with the additional requirement of more than 35 photomultiplier tubes firing in the BBC-S. Events that satisfy this trigger condition correspond roughly to the 5% most central event class. The use of this high-multiplicity trigger allows us to increase our central $p+$Au event sample size by a factor of 25. The ^{3}He + Au data set for this analysis were recorded during the 2014 run at RHIC, and comprises 1.6×10^9 MB events and 480×10^6 HM events. The HM trigger used in ^{3}He + Au is also based on the MB trigger, but with the additional requirement of more than 48 photomultiplier tubes firing in the BBC-S. The $d+$Au data set was recorded during the 2008 run, and comprises 1.56×10^9 MB events.

In this analysis, we select the 0%–5% most central events in all collision systems, where centrality classes are defined as percentiles of the total charged-particle multiplicity as measured in the BBC-S, following the procedure presented in [35]. We follow the identical analysis procedure that was previously used in ^{3}He + Au and $p+$Au collisions [4,14] to measure v_2 for inclusive charged hadrons. Namely, we measure v_2 for final-state single hadrons at midrapidity with respect to the event plane [36] of the collision, as follows:

$$v_2(p_T) = \frac{\left\langle \cos 2\left[\phi_{\text{Particle}}(p_T) - \Psi_2^{\text{FVTX-S}}\right]\right\rangle}{\text{Res}\left(\Psi_2^{\text{FVTX-S}}\right)}. \tag{1}$$

The event-plane angle is determined by the event flow vector Q_2 measured in the Au-going direction where the particle multiplicity is higher. The Q vectors are recentered according to the standard procedure described in [36]. The raw event-plane angle is estimated by

$$\Psi_n^{\text{raw}} = \text{atan2}\left(Q_2^y, Q_2^x\right)/2, \tag{2}$$

where Q_2^x and Q_2^y are the x and y projections of the flow vector. A standard flattening procedure described in [36] is applied to the Ψ_2^{raw} distributions to remove detector acceptance effects. The second-order event-plane angle $\Psi_2^{\text{FVTX-S}}$ is determined using the FVTX-S detector. Its resolution $\text{Res}(\Psi_2)$ is evaluated using the standard three-subevent method [36], correlating independent measurements made in the BBC-S, FVTX-S, and the central arms. The resolution of the event plane is found to be $\text{Res}(\Psi_2^{\text{FVTX-S},\,p+\text{Au}}) = 0.171$ in $p+$Au collisions, and $\text{Res}(\Psi_2^{\text{FVTX-S},\,^3\text{He+Au}}) = 0.274$ in ^{3}He + Au collisions. If the event plane is instead measured using the BBC-S detector, we obtain a lower resolution $\text{Res}(\Psi_2^{\text{BBC-S},\,p+\text{Au}}) = 0.062$ in $p+$Au and $\text{Res}(\Psi_2^{\text{BBC-S},\,^3\text{He+Au}}) = 0.070$ in ^{3}He + Au collisions.

The event-plane resolution depends on the particle multiplicity registered in the detectors used for event-plane determination, which results in better resolution in the FVTX-S than in the BBC-S.

III. SYSTEMATIC UNCERTAINTIES

We identify the following as the main sources of systematic uncertainty in the $v_2(p_T)$ measurement:

Background tracks from weak decays, photon conversions, and misreconstructed tracks. We estimate the magnitude of this uncertainty by narrowing the spatial matching windows of the tracks and the hits in the outermost layer of the PC, from 3σ to 2σ and comparing the resulting values of $v_2(p_T)$. The relative uncertainty in v_2 is 2% in both $p+\mathrm{Au}$ and $^3\mathrm{He}+\mathrm{Au}$ collisions.

Multiple collisions per bunch crossing. Also referred to as event pile-up, these are observed to occur at an average rate of 8% (4%–5%) in the centrality class of interest in $p+\mathrm{Au}$ ($^3\mathrm{He}+\mathrm{Au}$) collisions. We estimate the associated systematic uncertainty by analyzing low- and high-luminosity subsets of the data. The measured v_2 was found to decrease in events with higher pile-up rates, and an asymmetric systematic uncertainty of $^{+4}_{-0}\%$ was assigned in $p+\mathrm{Au}$, and $^{+5}_{-0}\%$ was assigned in $^3\mathrm{He}+\mathrm{Au}$ collisions.

Nonflow correlations from elementary processes. There are many sources of correlations among particles which enhance the measured v_2, yet are unrelated to collective flow, such as momentum conservation. We use a reference method previously employed in PHENIX analyses of small-system collectivity [14] to assign a p_T-dependent asymmetric uncertainty with a maximum value of $^{+0}_{-23}\%$ for the highest p_T bin in $p+\mathrm{Au}$ collisions. This can be compared to the corresponding values of $^{+0}_{-9}\%$ [3] and $^{+0}_{-7}\%$ [4] in $d+\mathrm{Au}$ and $^3\mathrm{He}+\mathrm{Au}$ collisions, respectively. The nonflow effect has a larger relative contribution in $p+\mathrm{Au}$ collisions due to the smaller multiplicity in this system.

Detector acceptance asymmetry. In $p+\mathrm{Au}$ collisions, there exists an asymmetry between the east ($\pi/2<\phi<3\pi/2$) and west ($-\pi/2<\phi<\pi/2$) acceptance of the detectors, originating from a 3.6 mrad offset between the beams at the collision point and the longitudinal axis of PHENIX. This offset is necessary to compare to $p+\mathrm{Au}$ collisions at the same momentum per nucleon. We account for this effect by performing a counter-rotation on every central arm track and detector element in the FVTX and the BBC, taking care to restore their azimuthal anisotropy by re-weighting. There remains a small residual asymmetry after applying these corrections in $p+\mathrm{Au}$. Meanwhile in $^3\mathrm{He}+\mathrm{Au}$ collisions this beam angle is negligible and we assign a value of 5% for this systematic uncertainty by taking the difference of v_2 when measured exclusively in the east or west arms in both $p+\mathrm{Au}$ and $^3\mathrm{He}+\mathrm{Au}$ collisions.

Event plane measured with different detectors. We observe the measured $v_2(p_T)$ to differ when using the event plane as determined using the BBC-S or the FVTX-S detectors. Despite the large difference in event-plane resolution in these two detectors, the differences in the measured $v_2(p_T)$ values are only of the order 3% in $p+\mathrm{Au}$, and 5% in $^3\mathrm{He}+\mathrm{Au}$ collisions, which demonstrates that the corrections for event-plane resolution are well understood.

TABLE I. Systematic uncertainties given as a percent of the v_2 measurement. Note that the nonflow contribution is p_T dependent and the quoted values correspond to the highest measured p_T.

Source	$p+\mathrm{Au}$	$^3\mathrm{He}+\mathrm{Au}$	Type
Track background	2%	2%	A
Event pile-up	$^{+4}_{-0}\%$	$^{+5}_{-0}\%$	B
Nonflow	$^{+0}_{-23}\%$	$^{+0}_{-7}\%$	B
Acceptance asymmetry	5%	5%	C
Event-plane detectors	3%	5%	C
Particle purity	2%	2%	B

Particle identification purity. The effect of particle identification purity on the measured v_2 values is evaluated by varying the width of particle selection windows in the mass-squared vs p_T space from 2σ to 1.5σ. The uncertainty is found to be at most 2% for both pions and protons in both collision systems.

Table I summarizes all these systematic uncertainties, categorized by type: A, point-to-point uncorrelated between p_T bins; B, point-to-point correlated between p_T bins; and C, overall normalization uncertainty in which all data points are scaled by the same multiplicative factor.

IV. RESULTS AND DISCUSSION

Figure 1 shows $v_2(p_T)$ for identified pions and protons in 0%–5% central $p+\mathrm{Au}$, $d+\mathrm{Au}$ [3], and $^3\mathrm{He}+\mathrm{Au}$ collisions. For both pions and protons the $v_2(p_T)$ values are higher in $d+\mathrm{Au}$ and $^3\mathrm{He}+\mathrm{Au}$ collisions than in $p+\mathrm{Au}$ collisions, as previously observed for inclusive charged hadrons [14]. These values follow the ordering of the initial geometric eccentricity $\varepsilon_2(p+\mathrm{Au})<\varepsilon_2(^3\mathrm{He}+\mathrm{Au})\approx\varepsilon_2(d+\mathrm{Au})$.

In the $d+\mathrm{Au}$ and $^3\mathrm{He}+\mathrm{Au}$ systems, there is a clear separation between the pion and proton v_2, with the pion v_2 being larger than the proton v_2 for $p_T\lesssim 1.5$ GeV/c and this order being reversed at higher p_T. In the $p+\mathrm{Au}$ system, the pion and proton $v_2(p_T)$ values show smaller overall splitting. The splitting pattern and the reversal of the mass ordering above $p_T\gtrsim 1.5$ GeV/c is qualitatively the same as has been observed in Au + Au collisions at $\sqrt{s_{NN}}=200$ GeV [20,37].

Figure 1 compares the measured $v_2(p_T)$ with hydrodynamic calculations using the SUPERSONIC model [38]. This model comprises standard Monte Carlo Glauber initial conditions followed by a viscous hydrodynamic expansion stage with $\eta/s=0.08$, Cooper-Frye hadronization at $T=170$ MeV, and a subsequent hadronic cascade code, B3D [39]. The SUPERSONIC model additionally incorporates pre-equilibrium dynamics via a calculation in the context of the anti–de Sitter-space/conformal-field-theory (AdS/CFT) correspondence [40–42]. These hydrodynamic calculations are matched to the measured charged-particle density at midrapidity in the 0%–5% centrality class for $d+\mathrm{Au}$ and $^3\mathrm{He}+\mathrm{Au}$ (i.e., $dN_{\mathrm{ch}}/d\eta=20.0$ and 27.0, respectively [43]). Because $dN_{\mathrm{ch}}/d\eta$ has not yet been measured in $p+\mathrm{Au}$ collisions, a value of $dN_{\mathrm{ch}}/d\eta=10.0$ was extrapolated for this system [38].

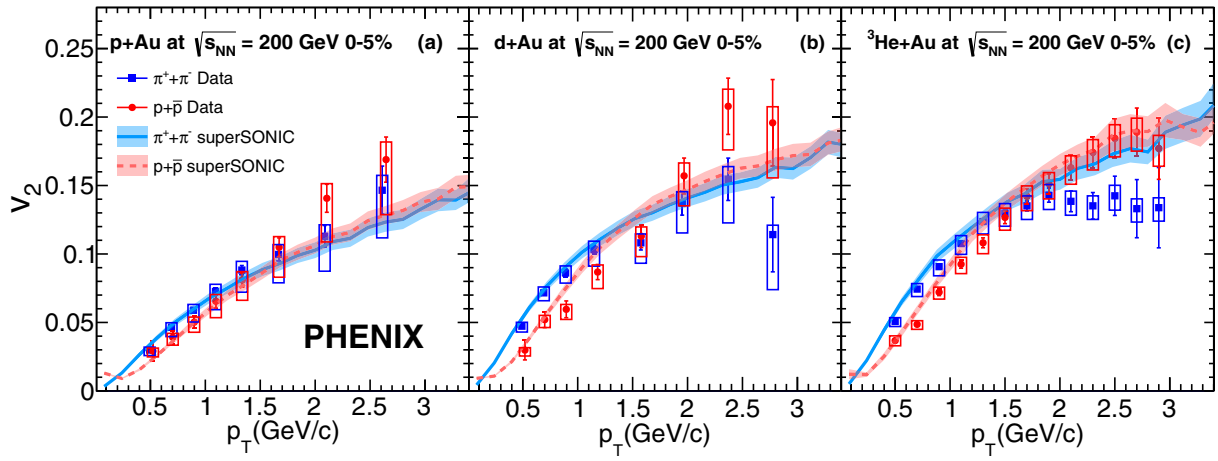


FIG. 1. Transverse momentum dependence of v_2 for identified pions and protons within $|\eta| < 0.35$ in 0%–5% central $p + \mathrm{Au}$, $d + \mathrm{Au}$ [3], and $^3\mathrm{He} + \mathrm{Au}$ collisions. The measurements are compared to hydrodynamic calculations using the SUPERSONIC model [38], matched to the same multiplicity at midrapidity as the data. Note that the data points shown include nonflow contributions, whose estimated magnitude is accounted for in the asymmetric systematic uncertainties.

We observe that the hydrodynamic calculations agree with the data within uncertainties at low p_T, but fail to describe the reversal of the pion and proton v_2 ordering for $p_T > 1.5$ GeV/c. Viscous hydrodynamic calculations similarly describe $\mathrm{Au} + \mathrm{Au}$ v_2 data at low p_T but do not match the strong reverse ordering at higher p_T. For $p_T < 1.5$ GeV/c, the mass splitting increases in going from $p + \mathrm{Au}$ to $d + \mathrm{Au}$ and $^3\mathrm{He} + \mathrm{Au}$ as also seen in the data. Within the context of hydrodynamic calculations, this is due to the increased radial flow and consequently larger velocity boost when going from the smaller and lower multiplicity systems to the larger and higher multiplicity systems.

In the case of ideal hydrodynamics, i.e., with zero viscosity, the v_2 values for all hadrons asymptotically approach each other at high p_T [44]. However, viscous effects and the incorporation of late-stage hadronic rescattering have the effect of lowering the high p_T v_2 values, more strongly so for pions. This can be seen in the SUPERSONIC calculations. However, the predicted high p_T splitting is much smaller than that seen in the $d + \mathrm{Au}$ and $^3\mathrm{He} + \mathrm{Au}$ data. It is in this high p_T region in $A + A$ collisions that proposals of hadronization via recombination [45] have been set forth to explain the v_2 splitting as well as the observation of enhanced baryon yields [46,47].

Figure 2 shows results from another viscous hydrodynamic calculation, iEBE-VISHNU [18]. The calculation includes event-by-event fluctuating initial conditions via Monte Carlo Glauber simulation and then viscous hydrodynamics starting at $\tau_0 = 0.6$ fm/c. The hydrodynamic evolution utilizes an $\eta/s = 0.08$ for RHIC energies and ends at $T = 155$ MeV. After that point, hadronization occurs and hadronic rescattering is implemented using URQMD 3.4 [48,49]. The calculation results with viscous hydrodynamics followed by hadronic rescattering show good agreement with the experimental data for all three small systems. Also shown are results with no hadronic rescattering that reveal almost no change in the v_2 for pions and protons for $p_T < 1.5$ GeV/c. The authors [18] conclude that hadronic

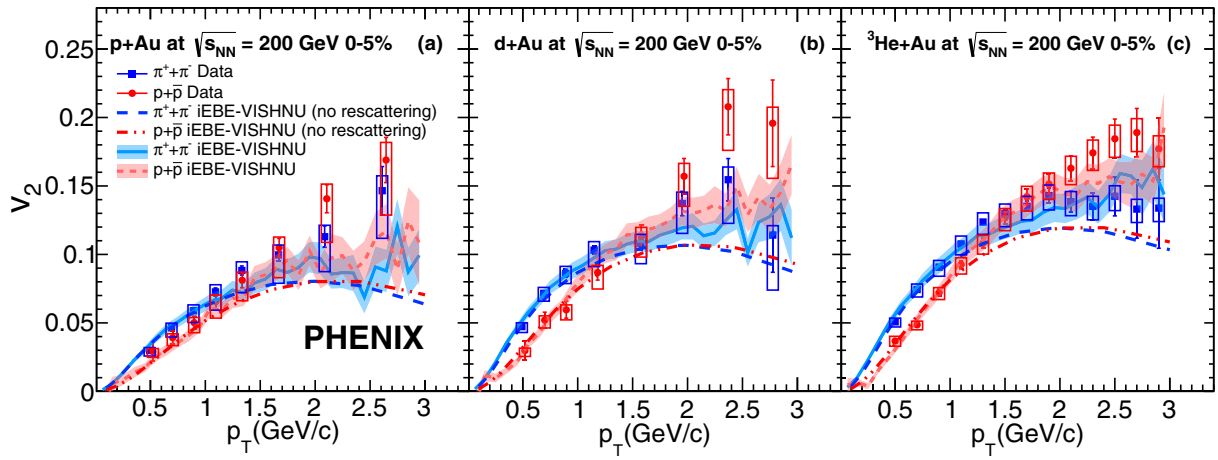


FIG. 2. Same as Fig. 1, but also shown are $v_2(p_T)$ calculations using the iEBE-VISHNU hydrodynamic model [18], illustrating the effect of hadronic rescattering on the mass-dependent v_2 values.

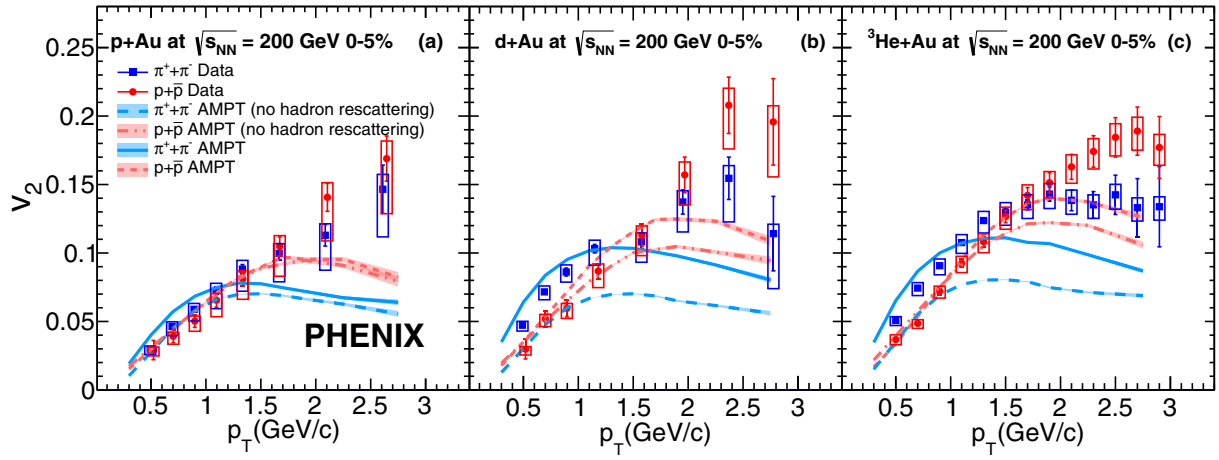


FIG. 3. Same as Fig. 1, but also shown are $v_2(p_T)$ transport model calculations using AMPT [23].

rescattering plays a modest but important role in the system development and particle species dependence of v_2 in these small systems.

Figure 3 compares the experimental data to transport model calculations of $v_2(p_T)$ for each system using AMPT [23]. The AMPT model has been successful in describing various features of small-system collectivity at RHIC and the LHC, over a wide range of collision energies [50–54]. It uses Monte Carlo Glauber initial conditions, and it models the evolution of the system via strings that melt into partons, followed by a succession of partonic scattering, spatial coalescence, and late-stage hadronic scattering implemented in ART [55]. We show results from the full AMPT time evolution with a partonic cross section $\sigma_{\text{part}} = 1.5$ mb, as well as results with the hadronic rescattering turned off. We calculate v_2 in central (i.e., $b < 2$ fm) AMPT events, relative to the parton participant plane. That is, the event plane is calculated using the initial coordinates of the partons, as they emerge from string melting at early times. We observe that the full AMPT describes the mass-dependent splitting in $d + \text{Au}$ and $^3\text{He} + \text{Au}$ for $p_T < 1.5$ GeV/c. In $p + \text{Au}$ collisions, the model results in a smaller mass splitting, which is reversed at high p_T yet below the experimental data. As noted in [24], AMPT generates significant v_2, and in particular mass splitting, in the hadronic rescattering stage. As also shown in Fig. 3, the results without rescattering have significantly lower v_2 values and almost no mass splitting for $p_T < 1$ GeV/c. At higher p_T, the feature of v_2 for protons being greater than pions remains without hadronic rescattering and is associated with the spatial coalescence implementation for hadronization.

Figure 4 shows the ratio of pion to proton $v_2(p_T)$ in all collision systems, with the corresponding theory curves overlaid. In the ratio, many systematic uncertainties cancel and thus one sees more precisely that the data exhibit a similar trend in all collision systems where pion v_2 is larger than proton v_2 for $p_T < 1.5$ GeV/c, with the order reversed at higher p_T. Linear fits on these ratios ranged from 0.5 to 3.0 GeV/c, which include both the statistical and the systematic uncertainties, yield slope values of -0.22 ± 0.07 in $p + \text{Au}$ collisions, -0.40 ± 0.07 in $d + \text{Au}$ collisions, and -0.34 ± 0.03 in $^3\text{He} + \text{Au}$ collisions. In this ratio, one can clearly see that SUPERSONIC, iEBE-VISHNU, and full AMPT modeling describe the mass splitting in $d + \text{Au}$ and $^3\text{He} + \text{Au}$ for $p_T < 1.5$ GeV/c. In the $p + \text{Au}$ case, it appears that the

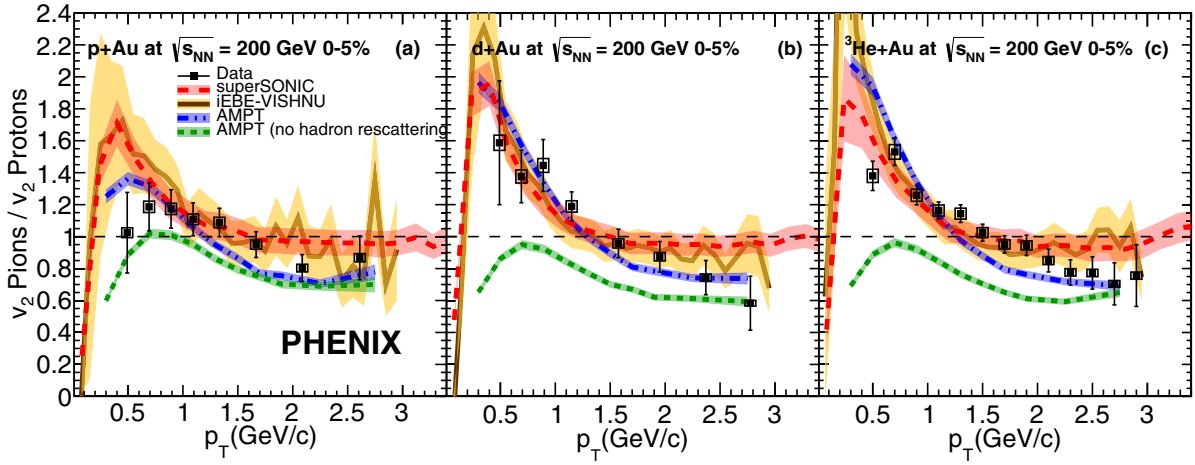


FIG. 4. Ratio of v_2^{pion} over v_2^{proton} in central 0%–5% (a) $p + \text{Au}$, (b) $d + \text{Au}$, and (c) $^3\text{He} + \text{Au}$ collisions at $\sqrt{s_{NN}} = 200$ GeV. Theoretical calculations from SUPERSONIC and AMPT are also shown.

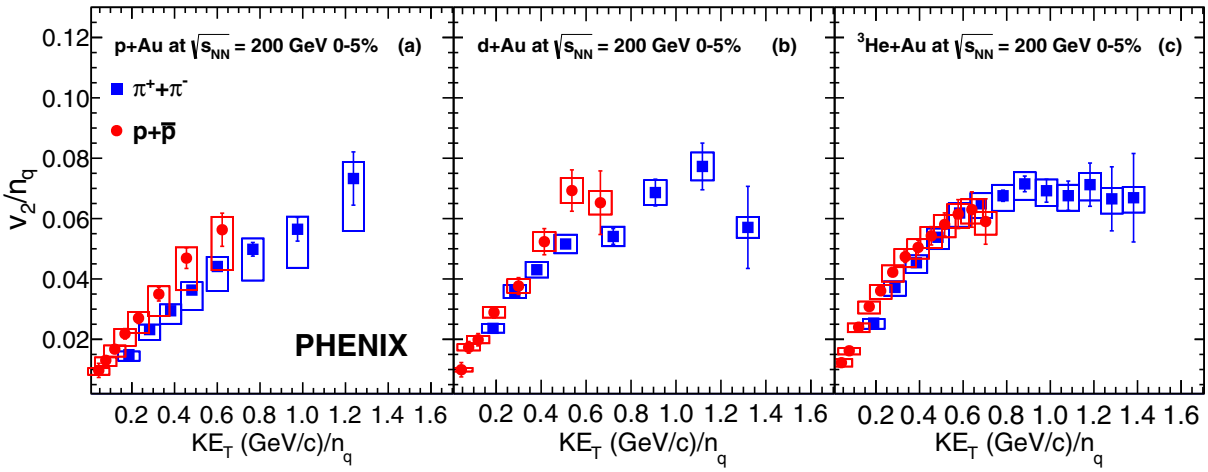


FIG. 5. Scaling of $v_2(p_T)$ with the number of constituent quarks in each hadron species, in 0%–5% central (a) $p+$Au, (b) $d+$Au, and (c) ^{3}He + Au collisions at $\sqrt{s_{NN}} = 200$ GeV.

calculations over predict the more modest splitting at the lowest measured $p_T = 0.5$ GeV/c. The results from AMPT without hadronic rescattering have very little mass splitting at low p_T in disagreement with the experimental data, particularly for $d+$Au and ^{3}He + Au collisions. Above the crossing point, SUPERSONIC, and iEBE-VISHNU predict nearly flat ratios, while AMPT describes the ratio of the v_2 values, but not their individual magnitudes. These differences may be attributed to the different hadronization mechanisms (e.g., if recombination is included) in the models.

The observation of a mass-dependent v_2 strengthens the case for associating small-system collectivity with the expansion of QGP droplets formed in these collisions, where the splitting can be understood in terms of the presence of a common radial flow field with anisotropic modulations driven by initial geometry. However, the theoretical calculations presented in this paper provide several alternative explanations of how the azimuthal anisotropies for different particle species may occur. For instance, in kinetic transport, parton scattering translates initial geometry into final-state momentum anisotropy, but it does not account for the observed mass splitting. Instead, this feature has been shown to arise solely from the hadronic rescattering stage where different hadrons have different inelastic cross sections [24]. There is more hadronic rescattering in ^{3}He + Au and $d+$Au than in $p+$Au for these central collisions because they have a higher particle density. It is interesting that this conclusion based on AMPT regarding the contribution of the hadronic rescattering stage is opposite to that reached using viscous hydrodynamics [18]. Differences in the hadronic scattering packages B3D [39] used in SUPERSONIC, URQMD [49] used in iEBE-VISHNU, and ART [23] used in AMPT warrant further investigation.

Finally, we return to the high p_T region where neither viscous hydrodynamics nor parton transport calculations match the data. Figure 5 shows the scaling of v_2 with constituent quarks as a function of transverse kinetic energy per quark $KE_T/n_q = (\sqrt{p_T^2 + m^2} - m)/n_q$, where m is the mass of the hadron and n_q represents the number of constituent quarks in the hadron. In all three systems, the v_2/n_q for pions and protons as a function of KE_T/n_q follow an approximate quark-number scaling. The same scaling was previously observed in $A+A$ collisions [20,37,56,57]. At intermediate p_T (1.5–4 GeV/c), the enhancement of baryons over mesons and the reversed mass ordering of v_2 in $A+A$ collisions have been interpreted in terms of hadronization via recombination. At even higher p_T, the scaling breaks down in noncentral $A+A$ collisions [58]. Similar to the observations in $A+A$, the enhancement of baryon over meson yields at intermediate p_T has been observed in central $d+$Au collisions [31], and now we also see the scaling with n_q in all three small collision systems. The scaling works better in $d+$Au and ^{3}He + Au collisions, where the projectile sizes and the particle densities are higher.

V. SUMMARY

We have presented results on the transverse momentum dependence of elliptic flow v_2 of identified pions and (anti)protons in central 0%–5% $p+$Au, $d+$Au, and ^{3}He + Au at $\sqrt{s_{NN}} = 200$ GeV. The $d+$Au and ^{3}He + Au data show a clear mass splitting with v_2 for pions larger than v_2 of protons for $p_T < 1.5$ GeV/c, and then a reversal of the ordering at higher p_T. The mass dependence is smaller in $p+$Au collisions than in $d+$Au and ^{3}He + Au collisions. Theoretical calculations, from viscous hydrodynamics and parton transport, yield a reasonable description of the low p_T mass splitting, despite having quite different mechanisms responsible for the observed mass dependence. At higher p_T, both models fail to describe the data, missing either the absolute value or the observed mass dependence. A scaling of v_2 with the number of constituent quarks, motivated by recombination, is observed in the data and is found to hold better in $d+$Au and ^{3}He + Au collisions, where the particle multiplicities are larger. All of these observations are qualitatively similar to previously measured effects in $A+A$ collisions. This again puts into sharp focus the question of whether the observations can be understood as arising from the same underlying physics, e.g., inviscid fluid expansion, in both large and small collisions systems. While alternative physics mechanisms have been

proposed, detailed comparisons with the experimental results are not yet available. This paper provides important constraints on the mass dependence of the particle correlations in small collision systems.

ACKNOWLEDGMENTS

We thank the staff of the Collider-Accelerator and Physics Departments at Brookhaven National Laboratory and the staff of the other PHENIX participating institutions for their vital contributions. We acknowledge support from the Office of Nuclear Physics in the Office of Science of the Department of Energy, the National Science Foundation, Abilene Christian University Research Council, Research Foundation of SUNY, and Dean of the College of Arts and Sciences, Vanderbilt University (U.S.A), Ministry of Education, Culture, Sports, Science, and Technology and the Japan Society for the Promotion of Science (Japan), Conselho Nacional de Desenvolvimento Científico e Tecnológico and Fundação de Amparo à Pesquisa do Estado de São Paulo (Brazil), Natural Science Foundation of China (People's Republic of China), Croatian Science Foundation and Ministry of Science and Education (Croatia), Ministry of Education, Youth and Sports (Czech Republic), Centre National de la Recherche Scientifique, Commissariat à l'Énergie Atomique, and Institut National de Physique Nucléaire et de Physique des Particules (France), Bundesministerium für Bildung und Forschung, Deutscher Akademischer Austausch Dienst, and Alexander von Humboldt Stiftung (Germany), J. Bolyai Research Scholarship, EFOP, the New National Excellence Program (ÚNKP), NKFIH, and OTKA (Hungary), Department of Atomic Energy and Department of Science and Technology (India), Israel Science Foundation (Israel), Basic Science Research Program through NRF of the Ministry of Education (Korea), Physics Department, Lahore University of Management Sciences (Pakistan), Ministry of Education and Science, Russian Academy of Sciences, Federal Agency of Atomic Energy (Russia), VR and Wallenberg Foundation (Sweden), the U.S. Civilian Research and Development Foundation for the Independent States of the Former Soviet Union, the Hungarian American Enterprise Scholarship Fund, the U.S.-Hungarian Fulbright Foundation, and the U.S.-Israel Binational Science Foundation.

APPENDIX: DATA TABLES

Tables II and III show the values of $v_2(p_T)$ for pions, kaons, and protons in central 0%–5% p + Au and ^{3}He + Au collisions at $\sqrt{s_{NN}} = 200$ GeV.

TABLE II. Values of $v_2(p_T)$ for pions, kaons, and protons in central 0%–5% p + Au collisions at $\sqrt{s_{NN}} = 200$ GeV.

	p_T range (GeV/c)	v_2	± stat	+ syst	− syst
$\pi^+ + \pi^-$	0.40–0.60	0.030	0.001	0.002	0.004
	0.60–0.80	0.046	0.002	0.003	0.007
	0.80–1.00	0.059	0.002	0.004	0.009
	1.00–1.20	0.073	0.003	0.005	0.013
	1.20–1.50	0.088	0.003	0.006	0.016
	1.50–1.90	0.100	0.005	0.007	0.021
	1.90–2.40	0.113	0.008	0.008	0.025
	2.40–3.00	0.147	0.018	0.011	0.035
$K^+ + K^-$	0.40–0.60	0.022	0.006	0.002	0.003
	0.60–0.80	0.037	0.005	0.003	0.005
	0.80–1.00	0.056	0.006	0.004	0.008
	1.00–1.20	0.068	0.007	0.005	0.012
	1.20–1.50	0.079	0.007	0.006	0.015
	1.50–1.90	0.091	0.009	0.007	0.019
$p + \bar{p}$	0.40–0.60	0.029	0.007	0.002	0.004
	0.60–0.80	0.039	0.005	0.003	0.006
	0.80–1.00	0.050	0.005	0.004	0.007
	1.00–1.20	0.066	0.005	0.005	0.012
	1.20–1.50	0.081	0.005	0.006	0.015
	1.50–1.90	0.105	0.007	0.008	0.022
	1.90–2.40	0.141	0.010	0.011	0.032
	2.40–3.00	0.169	0.016	0.013	0.040

TABLE III. Values of $v_2(p_T)$ for pions, kaons, and protons in central 0%–5% ^{3}He + Au collisions at $\sqrt{s_{NN}} = 200$ GeV.

	p_T range (GeV/c)	v_2	± stat	+ syst	− syst
$\pi^+ + \pi^-$	0.40–0.60	0.051	0.001	0.003	0.004
	0.60–0.80	0.074	0.001	0.004	0.005
	0.80–1.00	0.091	0.001	0.005	0.007
	1.00–1.20	0.108	0.002	0.006	0.008
	1.20–1.40	0.124	0.002	0.007	0.009
	1.40–1.60	0.130	0.003	0.007	0.010
	1.60–1.80	0.135	0.004	0.007	0.010
	1.80–2.00	0.143	0.005	0.008	0.011
	2.00–2.20	0.138	0.008	0.007	0.010
	2.20–2.40	0.135	0.010	0.007	0.010
	2.40–2.60	0.142	0.014	0.008	0.010
	2.60–2.80	0.133	0.021	0.007	0.010
	2.80–3.00	0.134	0.029	0.007	0.010
$K^+ + K^-$	0.40–0.60	0.041	0.003	0.002	0.003
	0.60–0.80	0.054	0.003	0.003	0.004
	0.80–1.00	0.077	0.003	0.004	0.006
	1.00–1.20	0.093	0.004	0.005	0.007
	1.20–1.40	0.109	0.005	0.006	0.008
	1.40–1.60	0.115	0.006	0.006	0.008
	1.60–1.80	0.123	0.007	0.007	0.009
	1.80–2.00	0.142	0.009	0.008	0.010
$p + \bar{p}$	0.40–0.60	0.037	0.002	0.003	0.004
	0.60–0.80	0.049	0.002	0.003	0.004
	0.80–1.00	0.072	0.002	0.004	0.005
	1.00–1.20	0.093	0.003	0.005	0.007
	1.20–1.40	0.108	0.004	0.006	0.008
	1.40–1.60	0.127	0.005	0.007	0.009
	1.60–1.80	0.142	0.006	0.008	0.010
	1.80–2.00	0.151	0.007	0.008	0.011
	2.00–2.20	0.163	0.009	0.009	0.012
	2.20–2.40	0.174	0.012	0.009	0.013
	2.40–2.60	0.184	0.014	0.010	0.014
	2.60–2.80	0.189	0.018	0.010	0.014
	2.80–3.00	0.177	0.023	0.010	0.013

[1] U. Heinz and R. Snellings, Collective flow and viscosity in relativistic heavy-ion collisions, Ann. Rev. Nucl. Part. Sci. **63**, 123 (2013).

[2] A. Adare *et al.* (PHENIX Collaboration), Quadrupole Anisotropy in Dihadron Azimuthal Correlations in Central d+Au Collisions at $\sqrt{s_{NN}} = 200$ GeV, Phys. Rev. Lett. **111**, 212301 (2013).

[3] A. Adare *et al.* (PHENIX Collaboration), Measurement of Long-Range Angular Correlation and Quadrupole Anisotropy of Pions and (Anti)protons in Central d + Au Collisions at $\sqrt{s_{NN}} =$ 200 GeV, Phys. Rev. Lett. **114**, 192301 (2015).

[4] A. Adare *et al.* (PHENIX Collaboration), Measurements of Elliptic and Triangular Flow in High-Multiplicity ^{3}He + Au Collisions at $\sqrt{s_{NN}} = 200$ GeV, Phys. Rev. Lett. **115**, 142301 (2015).

[5] B. Abelev *et al.* (ALICE Collaboration), Long-range angular correlations on the near and away side in p-Pb collisions at $\sqrt{s_{NN}} = 5.02$ TeV, Phys. Lett. B **719**, 29 (2013).

[6] G. Aad *et al.* (ATLAS Collaboration), Observation of Associated Near-Side and Away-Side Long-Range Correlations in $\sqrt{s_{NN}} =$ 5.02 TeV Proton-Lead Collisions with the ATLAS Detector, Phys. Rev. Lett. **110**, 182302 (2013).

[7] S. Chatrchyan *et al.* (CMS Collaboration), Observation of long-range, near-side angular correlations in p-Pb collisions at the LHC, Phys. Lett. B **718**, 795 (2013).

[8] V. Khachatryan *et al.* (CMS Collaboration), Measurement of Long-Range Near-Side Two-Particle Angular Correlations in pp Collisions at $\sqrt{s} = 13$ TeV, Phys. Rev. Lett. **116**, 172302 (2016).

[9] G. Aad *et al.* (ATLAS Collaboration), Observation of Long-Range Elliptic Azimuthal Anisotropies in $\sqrt{s} = 13$ and 2.76 TeV pp Collisions with the ATLAS Detector, Phys. Rev. Lett. **116**, 172301 (2016).

[10] Vardan Khachatryan *et al.* (CMS Collaboration), Observation of Long-Range Near-Side Angular Correlations in Proton-Proton Collisions at the LHC, J. High Energy Phys. 09 (2010) 091.

[11] V. Khachatryan *et al.* (CMS Collaboration), Evidence for collectivity in pp collisions at the LHC, Phys. Lett. B **765**, 193 (2017).

[12] K. Dusling and R. Venugopalan, Azimuthal Collimation of Long Range Rapidity Correlations by Strong Color Fields in High Multiplicity Hadron-Hadron Collisions, Phys. Rev. Lett. **108**, 262001 (2012).

[13] A. Ortiz Velasquez, P. Christiansen, E. Cuautle Flores, I. A. Maldonado Cervantes, and G. Paic, Color Reconnection and Flowlike Patterns in pp Collisions, Phys. Rev. Lett. **111**, 042001 (2013).

[14] C. Aidala *et al.* (PHENIX Collaboration), Measurement of long-range angular correlations and azimuthal anisotropies in high-multiplicity p + Au collisions at $\sqrt{s_{NN}} = 200$ GeV, Phys. Rev. C **95**, 034910 (2017).

[15] J. L. Nagle, A. Adare, S. Beckman, T. Koblesky, J. O. Koop, D. McGlinchey, P. Romatschke, J. Carlson, J. E. Lynn, and M. McCumber, Exploiting Intrinsic Triangular Geometry in Relativistic ^{3}He + Au Collisions to Disentangle Medium Properties, Phys. Rev. Lett. **113**, 112301 (2014).

[16] P. Bozek and W. Broniowski, Hydrodynamic modeling of ^{3}He + Au collisions at $\sqrt{s_{NN}} = 200$ GeV, Phys. Lett. B **747**, 135 (2015).

[17] B. Schenke and R. Venugopalan, Collective effects in light-heavy ion collisions, Nucl. Phys. A **931**, 1039 (2014).

[18] C. Shen, J. F. Paquet, G. S. Denicol, S. Jeon, and C. Gale, Collectivity and electromagnetic radiation in small systems, Phys. Rev. C **95**, 014906 (2017).

[19] R. D. Weller and P. Romatschke, One fluid to rule them all: Viscous hydrodynamic description of event-by-event central $p + p$, p + Pb and Pb + Pb collisions at $\sqrt{s} = 5.02$ TeV, Phys. Lett. B **774**, 351 (2017).

[20] S. S. Adler *et al.* (PHENIX Collaboration), Elliptic Flow of Identified Hadrons in Au + Au Collisions at $\sqrt{s_{NN}} = 200$ GeV, Phys. Rev. Lett. **91**, 182301 (2003).

[21] B. B. Abelev *et al.* (ALICE Collaboration), Long-range angular correlations of π, K and p in p-Pb collisions at $\sqrt{s_{\rm NN}} =$ 5.02 TeV, Phys. Lett. B **726**, 164 (2013).

[22] V. Khachatryan *et al.* (CMS Collaboration), Long-range two-particle correlations of strange hadrons with charged particles in p-Pb and PbPb collisions at LHC energies, Phys. Lett. B **742**, 200 (2015).

[23] Z. W. Lin, C. M. Ko, B. A. Li, B. Zhang, and S. Pal, Multiphase transport model for relativistic heavy ion collisions, Phys. Rev. C **72**, 064901 (2005).

[24] H. Li, L. He, Z. W. Lin, D. Molnar, F. Wang, and W. Xie, Origin of the mass splitting of elliptic anisotropy in a multiphase transport model, Phys. Rev. C **93**, 051901 (2016).

[25] B. Schenke, S. Schlichting, P. Tribedy, and R. Venugopalan, Mass Ordering of Spectra from Fragmentation of Saturated Gluon States in High Multiplicity Proton-Proton Collisions, Phys. Rev. Lett. **117**, 162301 (2016).

[26] K. Werner, M. Bleicher, B. Guiot, Iu. Karpenko, and T. Pierog, Evidence for Flow from Hydrodynamic Simulations of p-Pb Collisions at 5.02 TeV from v_2 Mass Splitting, Phys. Rev. Lett. **112**, 232301 (2014).

[27] P. Romatschke, Light-heavy-ion collisions: A window into pre-equilibrium QCD dynamics? Eur. Phys. J. C **75**, 305 (2015).

[28] K. Adcox *et al.* (PHENIX Collaboration), PHENIX detector overview, Nucl. Instrum. Meth. Phys. Res., Sec. A **499**, 469 (2003).

[29] C. Aidala *et al.*, The PHENIX Forward Silicon Vertex Detector, Nucl. Instrum. Meth. Phys. Res., Sec. A **755**, 44 (2014).

[30] M. Aizawa *et al.*, Phenix central arm particle id detectors, Nucl. Instrum. Methods Phys. Res., Sec. A **499**, 508 (2003).

[31] A. Adare *et al.* (PHENIX Collaboration), Spectra and ratios of identified particles in Au+Au and d+Au collisions at $\sqrt{s_{NN}} =$ 200 GeV, Phys. Rev. C **88**, 024906 (2013).

[32] GEANT3.2.1 Manual (CERN, Geneva, 1993); available at http://wwwasdoc.web.cern.ch/wwwasdoc/pdfdir/geant.pdf.5.

[33] A. Adare *et al.* (PHENIX Collaboration), Single electron yields from semileptonic charm and bottom hadron decays in Au + Au collisions at $\sqrt{s_{NN}} = 200$ GeV, Phys. Rev. C **93**, 034904 (2016).

[34] M. A. Allen *et al.*, PHENIX inner detectors, Nucl. Instrum. Methods Phys. Res., Sec. A **499**, 549 (2003).

[35] A. Adare *et al.* (PHENIX Collaboration), Centrality categorization for $R_{p(d)+\rm Au}$ in high-energy collisions, Phys. Rev. C **90**, 034902 (2014).

[36] A. M. Poskanzer and S. A. Voloshin, Methods for analyzing anisotropic flow in relativistic nuclear collisions, Phys. Rev. C **58**, 1671 (1998).

[37] C. Adler *et al.* (STAR Collaboration), Identified Particle Elliptic Flow in Au + Au Collisions at $\sqrt{s_{NN}} = 200$ GeV, Phys. Rev. Lett. **87**, 182301 (2001).

[38] M. Habich, J. L. Nagle, and P. Romatschke, Particle spectra and HBT radii for simulated central nuclear collisions of C + C,

Al + Al, Cu + Cu, Au + Au, and Pb + Pb from $\sqrt{s}$ = 62.4–2760 GeV, Eur. Phys. J. C **75**, 15 (2015).
[39] J. Novak, K. Novak, S. Pratt, J. Vredevoogd, C. E. Coleman-Smith, and R. L. Wolpert, Determining fundamental properties of matter created in ultrarelativistic heavy-ion collisions, Phys. Rev. C **89**, 034917 (2014).
[40] W. van der Schee, P. Romatschke, and S. Pratt, Fully Dynamical Simulation of Central Nuclear Collisions, Phys. Rev. Lett. **111**, 222302 (2013).
[41] P. M. Chesler and L. G. Yaffe, Holography and off-center collisions of localized shock waves, J. High Energy Phys. 10 (2015) 070.
[42] P. Romatschke and J. D. Hogg, Pre-Equilibrium Radial Flow from Central Shock-Wave Collisions in AdS5, J. High Energy Phys. 04 (2013) 048.
[43] A. Adare *et al.* (PHENIX Collaboration), Transverse energy production and charged-particle multiplicity at midrapidity in various systems from $\sqrt{s_{NN}}$ = 7.7 to 200 GeV, Phys. Rev. C **93**, 024901 (2016).
[44] P. Huovinen, P. F. Kolb, U. W. Heinz, P. V. Ruuskanen, and S. A. Voloshin, Radial and elliptic flow at RHIC: Further predictions, Phys. Lett. B **503**, 58 (2001).
[45] R. J. Fries, V. Greco, and P. Sorensen, Coalescence Models For Hadron Formation From Quark Gluon Plasma, Ann. Rev. Nucl. Part. Sci. **58**, 177 (2008).
[46] S. S. Adler *et al.* (PHENIX Collaboration), Scaling Properties of Proton and Anti-Proton Production in $\sqrt{s_{NN}}$ = 200 GeV Au+Au collisions, Phys. Rev. Lett. **91**, 172301 (2003).
[47] S. S. Adler *et al.* (PHENIX Collaboration), Identified charged particle spectra and yields in Au+Au collisions at $\sqrt{s_{NN}}$ = 200 GeV, Phys. Rev. C **69**, 034909 (2004).
[48] S. A. Bass *et al.*, Microscopic models for ultrarelativistic heavy ion collisions, Prog. Part. Nucl. Phys. **41**, 255 (1998).
[49] M. Bleicher *et al.*, Relativistic hadron hadron collisions in the ultrarelativistic quantum molecular dynamics model, J. Phys. G **25**, 1859 (1999).
[50] A. Adare *et al.* (PHENIX Collaboration), Measurements of directed, elliptic, and triangular flow in Cu + Au collisions at $\sqrt{s_{NN}}$ = 200 GeV, Phys. Rev. C **94**, 054910 (2016).
[51] J. D. Orjuela Koop, A. Adare, D. McGlinchey, and J. L. Nagle, Azimuthal anisotropy relative to the participant plane from a multiphase transport model in central p + Au, d + Au, and ^{3}He + Au collisions at $\sqrt{s_{NN}}$ = 200 GeV, Phys. Rev. C **92**, 054903 (2015).
[52] J. D. O. Koop, R. Belmont, P. Yin, and J. L. Nagle, Exploring the Beam Energy Dependence of Flow-Like Signatures in Small System d + Au Collisions, Phys. Rev. C **93**, 044910 (2016).
[53] G. L. Ma and Z. W. Lin, Predictions for $\sqrt{s_{NN}}$ = 5.02 TeV Pb + Pb Collisions from a Multi-Phase Transport Model, Phys. Rev. C **93**, 054911 (2016).
[54] G. Ma and A. Bzdak, Long-range azimuthal correlations in proton-proton and proton-nucleus collisions from the incoherent scattering of partons, Phys. Lett. B **739**, 209 (2014).
[55] B. A. Li and C. M. Ko, Formation of superdense hadronic matter in high energy heavy-ion collisions, Phys. Rev. C **52**, 2037 (1995).
[56] A. Adare *et al.* (PHENIX Collaboration), Scaling Properties of Azimuthal Anisotropy in Au+Au and Cu+Cu Collisions at $\sqrt{s_{NN}}$ = 200 GeV, Phys. Rev. Lett. **98**, 162301 (2007).
[57] John Adams *et al.* (STAR Collaboration), Particle Type Dependence of Azimuthal Anisotropy and Nuclear Modification of Particle Production in Au + Au Collisions at $\sqrt{s_{NN}}$ = 200 GeV, Phys. Rev. Lett. **92**, 052302 (2004).
[58] A. Adare *et al.* (PHENIX Collaboration), Deviation from quark-number scaling of the anisotropy parameter v_2 of pions, kaons, and protons in Au+Au collisions at $\sqrt{s_{NN}}$ = 200 GeV, Phys. Rev. C **85**, 064914 (2012).